

Supplementary Information for:

The impact of system integration on system costs of a neighborhood energy- and watersystem

Els van der Roest ^{1,2*}, Theo Fens ³, Martin Bloemendal ^{1,2}, Stijn Beernink ^{1,2}, Jan Peter van der Hoek ^{2,4} and Ad J.M. van Wijk ^{1,5}

¹ KWR Water Research Institute, Department of Sustainability & Transitions, Groningenhaven 7, 3430 BB Nieuwegein, The Netherlands.

² Faculty of Civil Engineering and Geosciences Delft University of Technology, Stevinweg 1, 2638 CN Delft, The Netherlands

³ Economics of Infrastructures section, Delft University of Technology, Jaffalaan 5, 2638 BX Delft, The Netherlands

⁴ Waternet, Korte Oudekerkerdijk 7, 1096 AC Amsterdam, The Netherlands

⁵ Department of Process and Energy, Delft University of Technology, Leeghwaterstraat 39, 2638 CB Delft, The Netherlands

* Corresponding author at: E.vanderRoest@tudelft.nl

Modelling methodology

In this section, for each system element mentioned in Figure 1 (of the main publication), a description of how this element is modelled is given.

S. 1. Supply

S.1.1. Rainwater

Precipitation data from hourly weather data (mm/hr or L/m²/hr) are converted to cubic meters of precipitation per hour according to the following formula:

$$v_{rain_i} = \frac{v_{precipitation} A_{surface} \cos(\beta)}{1000}$$

With v_{rain_i} the total amount of rainwater in m³/hr on specific surface i , which can be a roof or a solar park. $v_{precipitation}$ represents precipitation data in L/m²/hr, $A_{surface}$ the total surface area of either roofs or solar panels in m² and $\cos(\beta)$ the angle of the roof or solar panels.

S.1.2. Surface water

Hourly data on surface water temperatures are used as an input for the model. The surface water can only be used as a heat source when the temperature is above 14 °C. Between 14 °C – 18 °C, the water is cooled with 3 °C and above 18 °C with 6 °C, based on a report with 13 business cases for surface water thermal energy systems [1]. At the start of the heat storage season, the temperature difference is smaller to reduce ecological effects. In summer the effect of cooling the surface water is positive, because of higher oxygen content and a decreased chance for the development of algae, botulism and smell [1,2]. In general, this means that in the Netherlands, surface water can be used as a heat source for five months, from May up until September.

S.1.3. Solar PV

The energy production for both rooftop PV and solar parks is calculated at an hourly basis with the equations as used in the HOMER (Hybrid Optimization of Multiple Energy Resources), whereby the temperature effect is taken into account [3]. The temperature coefficient is chosen at 0.41%/°C and the nominal operating cell temperature (NOCT) is set at 45 °C. Furthermore, we assume a 10% loss factor for losses due to shadow, dust, waste transformation, and fixed linear derating factor to 81% of the original efficiency over 25 years.

S.1.4. Wind

Wind energy is not part of the scenarios calculated in this paper but is included in the Power-to-X model, hence we do include it in the methodology. For wind turbine energy output, wind speed data at ground level (in general 10 m height) are transformed to wind speed at 60 meters height according to Eq (S.1).

$$u_{h_2} = \frac{\ln(h_2/z_0)}{\ln(h_{meter}/z_0)} \cdot u_{meter} \quad (S.1)$$

Where u_{h_2} (m/s) is the wind speed at a height h_2 (in m, max. 60m), u_{meter} is the wind speed at reference height (m/s), h_{hub} is the hub height of a selected turbine in m and h_{meter} the reference height of the weather station in m (often 10 m). z_0 represents the surface roughness (in m). The height of 60m is called the blending height, as this is the point where the effects from the Earth's surface (represented by the roughness factor) are not influencing the wind speed anymore [4]. From this point onwards, the power law is used to calculate the wind speed from 60m (h_1) to hub height (h_2), see Eq (S.2):

$$u_{h_2} = u_{h_1} \cdot \left(\frac{h_2}{h_1}\right)^\alpha \quad (S.2)$$

Where α is a constant value that differs for land and sea, with the standard value for land being 0.143. u_{h_2} is the wind speed at hub height (in m/s).

S.2. Conversion technologies

S.2.1. Rainwater treatment

The rainwater is cleaned by a sieve and self-cleaning filter. A small part of the water is purified further by the reverse osmosis system (RO) and stored in short-term water storage (tank). The remaining filtered rainwater water is stored in the subsurface (without reversed osmosis treatment). When the electrolyser has a water demand, water from the RO storage tank is purified further by a continuous electro deionisation system (CEDI) [5]. Water demand for other purposes is either fulfilled directly with water from the underground storage or first treated by the RO installation, depending on the purpose. A picture of the system layout can be found in van der Roest et al. [6], p.5. For the different treatment steps, the water recovery is defined in Table 1. The energy use of the water treatment system is mainly defined by the energy use of pumps, according to:

$$E_{pump} = \frac{f_{pump} \Delta p}{3600 \eta} \quad (S.3)$$

With E_{pump} the energy use of the pump in kWh, f_{pump} the flow through the pump in m³/hr, Δp the feed versus outflow pressure difference in kPa and η the efficiency of the pump.

Table 1 Water system components and efficiencies

	Water recovery	Pressure difference (kPa)	Pump efficiency
Sieve	98%	-	-
Self cleaning filter	98%	250	60%
Water storage pump	100%	100	60%
Reverse osmosis system	90%	700	80%
CEDI	95%	300	60%

S.2.2. Electrolyser

Electrolysers convert electricity to hydrogen and are available in different variations. In this paper, we have chosen to look at a proton exchange membrane (PEM) electrolyser. PEM produces hydrogen at 30 bar pressure and with a very high quality (5.0, meaning 99.999% pure hydrogen), which is beneficial when the hydrogen is (partly) used for mobility purposes. The efficiency has a negative correlation with the load, therefore we use an efficiency curve that varies with the load, based on experimental data from [7] but adapted for 2030, which is shown in Figure 1. The average efficiency (HHV) is set at 80% at 90% load, or 50 kWh/kg which is the expected efficiency of a PEM electrolyser for 2030 [8].

Because a PEM electrolyser has an operating temperature of 50-80°C, the heat from the electrolyser is coupled to the heat storage system. This means that the electrolyser has a water-based cooling system with a heat exchanger that is coupled to the heat distribution system. We assume that 80% of the heat can be recovered. In this way, the total efficiency of the electrolyser increases from about 80% to 94%.

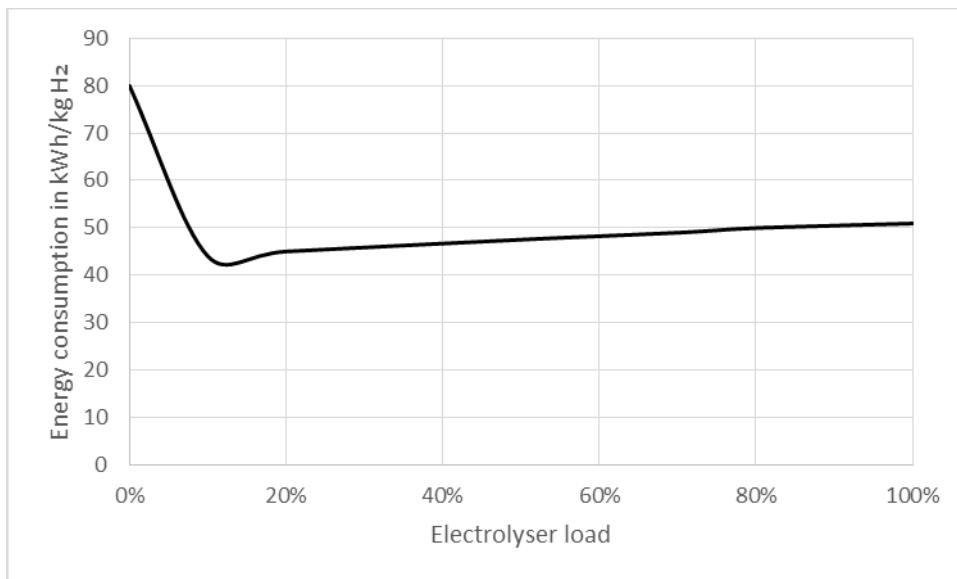


Figure 1 PEM Electrolyser efficiency versus load, based on[7]

S.2.3. Industrial heat pump

The heat pump converts power to heat of 50°C with surface water as a heat source. The energy consumption of a heat pump depends on the coefficient of performance (COP) which is based on industrial scale heat pump software DORIN [9] and defined as:

$$COP_{HP} = 0.0028 (T_{HP,cond} - T_{HP,evap})^2 - 0.3276 (T_{HP,cond} - T_{HP,evap}) + 13.021 \quad (S.4)$$

With $T_{HP,cond}$ the desired outflow temperature of the heat pump at the condenser side plus 5°C, and $T_{HP,evap}$ the inlet temperature of the heat pump minus 6°C for a conservative estimation of the COP of the heat pump, also taking into account losses over heat exchangers in the heat pump.

S.2.4. Household heat pumps

Because of the different options for household heating, there are different types of household heat pumps applied in the model.

First, a distinction is made between air sourced heat pumps (ASHP) and water sourced heat pumps (WSHP), with COP formulas from Ruhnau, Hirth and Praktiknjo [10].

$$COP_{ASHP} = 6.08 - 0.09 \cdot (T_{out} - T_{in}) + 0.0005 (T_{out} - T_{in})^2 \quad (S.5)$$

$$COP_{WSHP} = 9.97 - 0.02 \cdot (T_{out} - T_{in}) + 0.0012 (T_{out} - T_{in})^2 \quad (S.6)$$

With T_{out} being 35 °C for space heating meant for floor/low-temperature heating systems and T_{out} being 65 °C for domestic hot water.

For the air sourced heat pump, T_{in} is the outside air temperature.

In the case of hydrogen-hybrid heating, the heat pump supplies only space heat when the outside temperature is above -5°C. For domestic hot water and space heating when the outside temperature is below -5°C, the hydrogen boiler is used.

Lastly, we have the option of a water sourced booster heat pump that is installed to provide only domestic hot water, with the temperature of the district heating network as input temperature T_{in} .

S.2.5. Hydrogen boiler

When a hydrogen boiler is installed, it is always used together with a heat pump (see S.2.4). It provides domestic hot water and space heating when the outside temperature is below -5°C. The amount of hydrogen needed for heating (in kg) is calculated according to:

$$H_{2,heating} = \frac{E_{heatdem}}{\eta_{H2,boiler} \cdot E_{H2}} \quad (S.7)$$

With $E_{heatdem}$ the heat demand in kWh, $\eta_{H2,boiler}$ the efficiency of the hydrogen boiler, here set to 98% and E_{H2} the energy content of hydrogen set at 39.4 kWh/kg (HHV-based, and used through all model calculations).

S.2.6. Heat exchanger

The heat exchangers are modelled with a counter-current flow and a fixed heat loss of 1.5 °C.

S.2.7. Fuel Cell

A fuel cell is used to convert stored hydrogen to electricity as well as heat. We have chosen for a PEMFC because the operating temperature range matches well with the heat storage temperature and the installation has high responsiveness. The efficiency of PEMFC is currently not much higher than 50%, but for 2030 we assume a value of 60% efficiency which is seen as the

future potential [8]. Similar to the electrolyser, we assume that 80% of the heat can be used by the heat storage system.

S.3.Storage

S.3.1. Rainwater

Rainwater could be stored in an aquifer for later use with a recovery efficiency of 70% [11]. To pump water in and out of the aquifer, a pressure difference of 100kPa is assumed and a pump efficiency of 60%.

S.3.2. Hydrogen

Hydrogen is stored at central places in salt caverns and transported to the neighbourhood by (existing) gas infrastructure. There is enough room for hydrogen storage in salt caverns, in the Netherlands, there is 43.3 TWh (14.5 billion m³) estimated storage capacity potential in salt caverns on land, which is considerable compared to the current natural gas storage capacity of 145 billion m³ in Europe [12]. On average, a salt cavern is located at a depth of >500 m, mostly between 1000-2000 m and has a volume of about 500.000 – 750.000 m³ [13]. A cavern has a height of approximately 300-400m and a width of 50-80m [12,13]. The storage pressure is 80 bar (empty, only cushion gas) and 180 bar (storage is full) [14]. To store hydrogen in the salt cavern, compression to about 200 bars is needed (ca 1.5 kWh/kg H₂ for compression to 200 bar [15]). We assume no molecule losses occurred during storage.

S.3.3. High-temperature aquifer thermal storage (HT-ATES)

We include seasonal heat storage in the model in the form of a high-temperature aquifer thermal storage system. For the dynamics of groundwater flow, convection and conduction losses, a dedicated SEAWAT v4[16] model that couples MODFLOW [17] and MT3DMS [18] is used. There is a daily exchange of data between the hourly Power-to-X model and the HT-ATES (MODFLOW) model. Every day, the current temperature of both the warm and the hot well are returned to the hourly model. These values are then used for the next 24 hours of hourly runs before they are updated again.

The outlet temperature of the heat pump is set at 50°C, which means water is infiltrated at 48.5°C in the hot well. During winter, the temperature of the hot well is decreasing slowly. To use the HT-ATES most efficiently, we designed different heat pump modes.

- Heat charging - In this mode, surface water is used as input temperature at the evaporator side of the heat pump, while the water at the condenser side (50°C) is exchanged via a heat exchanger with water that is extracted from the warm well (12-26.5 °C) and infiltrated (at 48.5 °C) to the hot well.
- Direct heat delivery – Water from the hot well (43- 48.5°C) is exchanged via a heat exchanger with the return flow of the DHN (25°C). The DHN flow is thereby heated up (41.5-47 °C) and the water from the hot well is injected in the warm well (at 26.5 °C) after heat exchange.
- Heat charging and delivery – A combination of the two modes described above. The heat produced by the heat pump is first delivered

to the (warm) distributor of the DHN, but the share of the heat that is not necessary to fulfil the heat demand is exchanged with the HT-ATES system.

- Heat delivery under the threshold ($T_{\text{hot well}} = 43\text{ }^{\circ}\text{C}$) - If the temperature of the hot well reaches the threshold value ($43\text{ }^{\circ}\text{C}$) a different heat pump mode will start. In this mode, there is still exchange with the return pipe of the DHN (via heat exchanger nr. 1), but the temperature is not high enough to provide direct household heating. Therefore, the heat pump is used to upgrade the heat flow with the (warmed up) Retour flow from the DHN at the condenser side. At the evaporator side, the - the already cooled- flow from the hot well is exchanged via a second heat exchanger with a loop that goes to the evaporator side of the heat pump (Figure S2). In this way, the COP of the heat pump stays high and heat is produced efficiently. Moreover, the temperature of the hot well is lowered, which helps to maintain a quite constant ΔT between the wells and therefore has a positive effect on the system efficiency.
- HT-ATES shut off ($T_{\text{hot well}} < 30\text{ }^{\circ}\text{C}$) - When the temperature of the hot well decreases below $30\text{ }^{\circ}\text{C}$, the HT-ATES system stops working to prevent the hot well from cooling off further. If the hot well becomes too cold, there is a high risk that the hot well is not able to deliver enough heat in the next winter. Therefore, if the hot well temperature decreases below $30\text{ }^{\circ}\text{C}$, heat has to be provided from a different source. If this happens, it is generally at the end of the winter so it could perhaps be possible to use the surface water as a source again. For now, we have assumed that heat is in this case produced from a source with a temperature of $12\text{ }^{\circ}\text{C}$. When the HT-ATES system had to be shut off for more than 5% of the time, the system has to be redesigned with a larger heat pump.

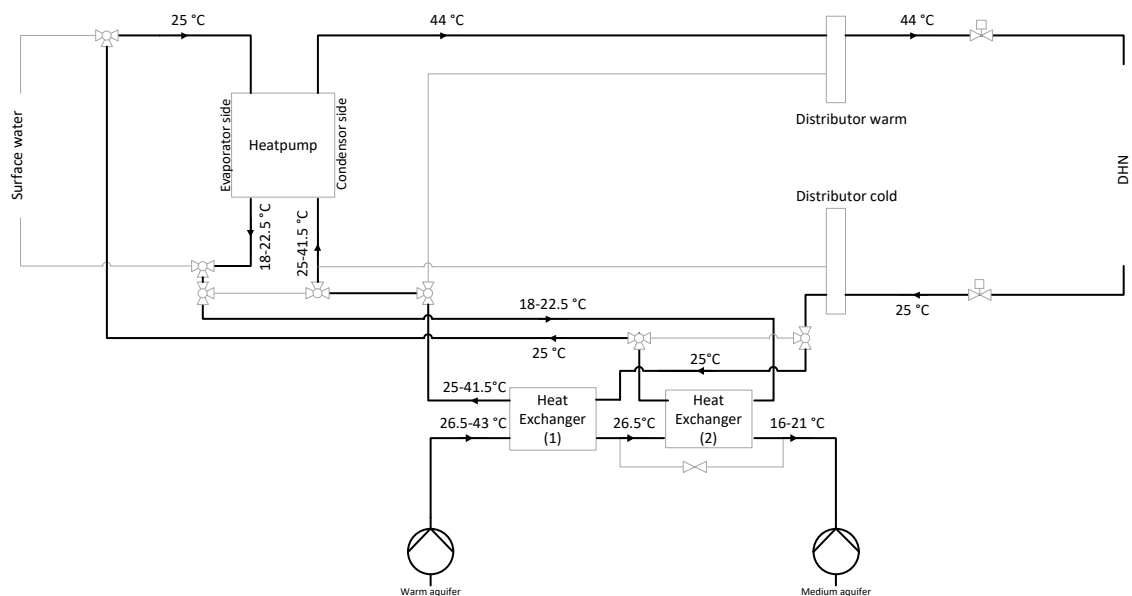


Figure S2 Heat pump mode when the HT-ATES is functioning between 30-43 °C, The flow from the hot aquifer does first exchange heat with the return flow of the DHN, and afterwards with the evaporator

side of the heat pump, to ensure efficient use of the heat. In grey, alternative flows are shown for other heat pump modes, such as charging the hot well and direct discharging of the hot well.

For this paper, the HT-ATES system parameters are based on a specific case of Nieuwegein. We model three layers, specifications are given in Table 2. The two wells are modelled separately, but do communicate by the volume and temperature of flows that flow from one well to the other. More details on the modelling methodology can be found in the report of the Power-to-X concept [19], appendix V.

Table 2 Specifications of the layers modelled for the HT-ATES system

Layer	zTop (m)	zBottom (m)	Kh (mD) Horizontal permeability	Kv (mD) Vertical permeability	porosity
1	0	-25	0.05	0.01	0.3
2	-25	-55	35	7	0.3
3	-55	-70	0.05	0.01	0.3

We have chosen to model the heat storage system in a steady-state phase. This means the model is first run from a 'cold start' with the subsurface (water) temperature at 12°C. We run the model for five years to let the system reach equilibrium and then save the status of the HT-ATES system to use in a subsequent model run. In this way, we create a fairer comparison between different scenarios (with and without heat storage) later on.

The yearly heat recovery efficiency in % (η) is calculated by:

$$\eta = \frac{\sum_0^{8760} \Delta T \cdot V_{out} \cdot c_w}{\sum_0^{8760} \Delta T \cdot V_{in} \cdot c_w} \cdot 100\% \quad (\text{S.8})$$

$$\Delta T_{system} = \hat{T}_{hot} - \hat{T}_{warm} \quad (\text{S.9})$$

$$\Delta T_{hot\ well} = \hat{T}_{hot} - T_{amb} \quad (\text{S.10})$$

$$\Delta T_{warm\ well} = \hat{T}_{warm} - T_{amb} \quad (\text{S.11})$$

With \hat{T}_{hot} the moving average temperature of the hot well (in °C) and \hat{T}_{warm} the moving average temperature of the warm well of the HT-ATES system (in °C). T_{amb} is the background ambient temperature in the aquifer (12°C). V is the flow (volume) of the water in m³/h in or out of the hot well and c_w is the heat capacity of water (4180 kJ/m³/K). Depending on the applied ΔT in formula S.8, either the recovery efficiency of the total HT-ATES system, the hot well or the warm well is calculated.

S.3.4. Electricity (Battery storage)

For short term electricity storage, a large scale battery can be added to the system. The battery was modelled with 95% efficiency (one-way) [20,21], the

maximum depth of discharge (DoD) is 90% and the maximum charge/discharge capacity is 25% (C-rate of 4) [21].

S.4. Distribution

S.4.1. Electricity grid

When electricity is exported from the neighbourhood (0.4 kV) to the grid (10 kV) or the other way around, a transformer efficiency of 98% was assumed. Within the neighbourhood, no losses for conversion are taken into account. This is a simplification but partly justified because we assume that most installations in 2030 will have a DC connection, which saves the conversion from DC to AC and back in between i.e. a solar park, battery and electrolyser.

S.4.2. District heating network

For the distribution of heat in the neighbourhood, the heat loss in the district heating network (DHN) is calculated based on the NEN-norms for district heating [22]. We have chosen to calculate the heat loss in °C for the average flow and the complete length of the DHN, so for the last house on the network. The ΔT of the heat loss (including the loss over the heat exchanger) is then used to calculate the heat loss per hour (in GJ) using the hourly flow in the DHN related to the total heat demand of all houses in the neighbourhood (based on 44°C inlet temperature and 25°C return temperature). For pump energy, a value 2% of the heat generated is taken into account [23].

S.4.3. Hydrogen distribution network

For hydrogen transport, we look at reuse of the existing gas network, which is suitable for hydrogen transport after some modifications [24,25], mainly to pipe connectors and flow meters [26]. We assume no losses occur during distribution.

S.4.4. Hydrogen fuelling station

A hydrogen fuelling station (HFS) will be placed outside the neighbourhood. Ideally, it is close to the hydrogen infrastructure so it receives hydrogen directly at the station. Otherwise, hydrogen has to be transported with trucks to the fuelling station. For now, we assumed that hydrogen can be transported to the HFS by pipeline, which means it needs to be pressurized from 30 bars (pipeline) to 880 bars (to be able to refuel cars at 700 bars). This energy use is outside of the scope of this paper. The costs of the HFS were not taken into account separately in this paper, as the HFS will not be placed in the neighbourhood itself and a fuelling station has a number of users that exceeds the size of the neighbourhood. The costs for the fuelling station will be part of the price of hydrogen paid at the HFS itself and are expected to be 0.8-1.6 €/kg [25].

S.5. Energy Demand

S.5.1. Cars hydrogen demand

The neighbourhood will have a HFS nearby for refuelling the hydrogen cars from their (and other) neighbourhoods. The tank pattern shown in Figure 3

was used in the model. The hydrogen demand can vary per scenario, which is the reason that percentages are shown here. To ensure variability over time, a 10% noise is applied to the fuelling pattern.

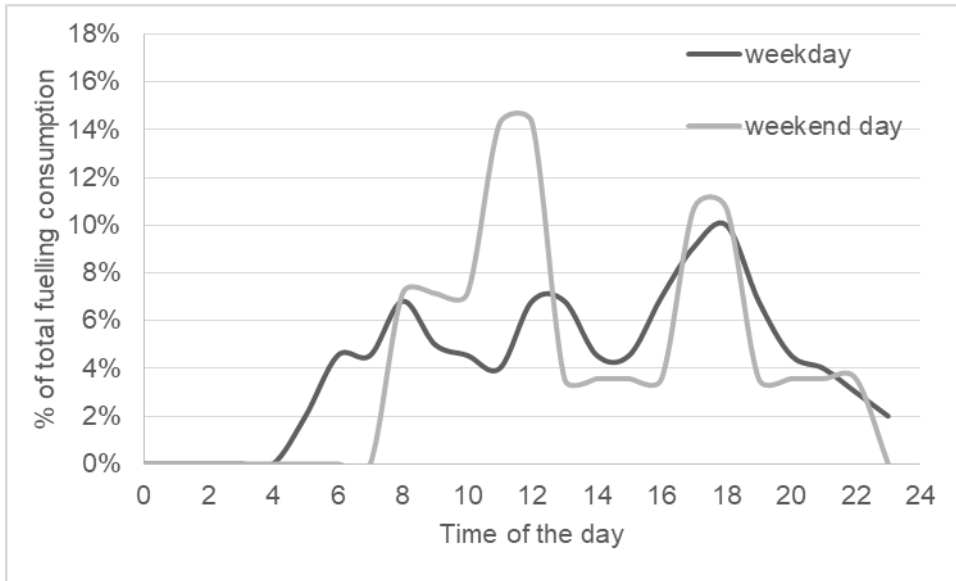


Figure 3 Daily fuelling pattern for hydrogen cars

S.5.2. Heat demand

S.5.2.1. Space heat demand

The model has a top-down approach regarding heat demand, which means that the total yearly heat demand is set as a model parameter at the start of a model run. The yearly heat demand varies per building type. In the model, the heat demand is distributed over time according to the degree-day method that is explained with:

$$HDH_i = (T_{base} - T_{outside,i}) \cdot f_{seasonal} \quad (S.10)$$

Whereby the amount of heat degree hours (HDH) in hour i is given by the difference between the outside temperature at which a house should be heated (T_{base}), here set on 14°C , and $T_{outside,i}$ the outside temperature at hour i , both in $^{\circ}\text{C}$. The weighting factor $f_{seasonal}$ takes into account the solar irradiation in the house and is 0.8 from April to September, 1.0 in March and October and 1.2 from November to February. One of the pitfalls when using the degree-day method is that intermittent heating (lower the thermostat temperature at night) is not represented with this method. However, in our neighbourhood, we expect the heating system to work at a lower temperature, such as floor heating. With these systems, the assumption that a constant temperature level is maintained during night and day is justified.

In the model, a top-down approach is applied, with a fixed yearly heat demand which is distributed over the year utilizing the total amount of heat degree hours. First, a fraction of the space heat demand per degree hour is calculated ($f_{\text{demand,space heat}}$ in kWh/hr) according to Eq (S.11) and then this fraction is

used to calculate the heat demand in every hourly time step by multiplying the factor by the hourly value for heat degree hours as shown in Eq (S.12).

$$f_{demand,spaceheat} = \frac{E_{spaceheat,total}(kWh)}{\sum_{i=1}^{8760} HDH_i} \quad (S.11)$$

$$Q_{spaceheat,i}(kWh/h) = HDH_i \cdot f_{demand,heat} \quad (S.12)$$

Where $E_{space\ heat,total}$ is the total space heat demand of the neighbourhood in kWh and $Q_{space\ heat,i}$ is the heat demand in the neighbourhood in a certain hour i , in kWh.

S.5.2.2. Domestic hot water heating demand

The heat demand of a household exists not only of space heating demand but includes domestic hot water (at 65°C) as well. The domestic hot water demand is not related to the outside temperature as is the space heating demand. Therefore, a domestic hot water demand pattern with peaks for showering both in the morning and night was used from [27] (p.27). A 10% noise is applied to the daily domestic hot water demand pattern to ensure some variability in the demand.

S.5.3. Electricity demand

S.5.3.1. Household electricity demand

The electricity demand of households is a parameter that depends on the scenario used, as it depends on the building type. The yearly electricity demand is distributed over the year with 15-minute data from the Dutch Institute for Energy Data Exchange (NEDU, *Nederlandse Energie Uitwisseling Data*) [28]. The E1A profile for households was used, which varies both seasonally and daily.

We assume that all houses cook on electricity, which is not common at the moment in the Netherlands as 78% of the households uses natural gas for cooking [29]. Electric cooking is thus not included in the average electricity use profiles and is therefore added to the yearly electricity demand with a separate demand pattern, based on a report from a Dutch consulting agency [30]. To ensure variability over time, a noise of 10% is applied to the electric cooking pattern.

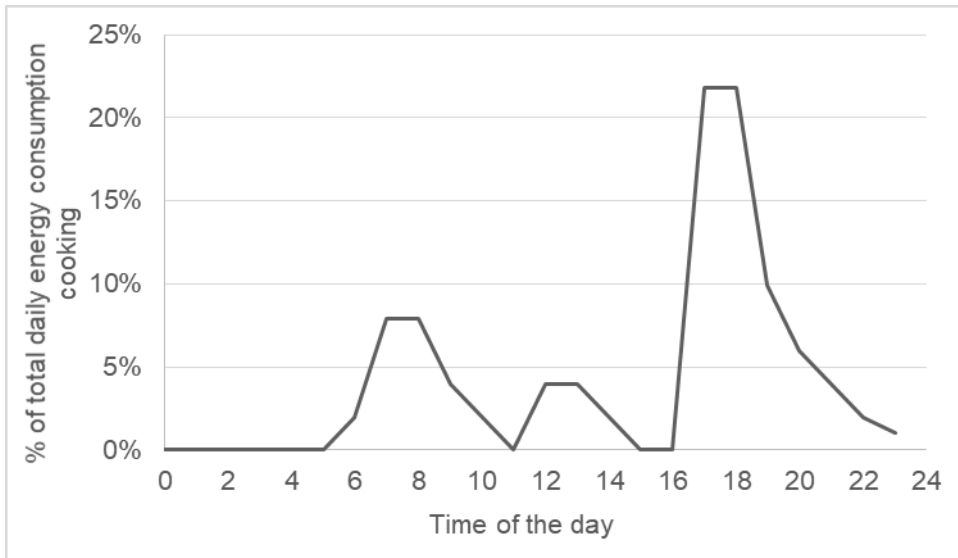


Figure 4 Daily pattern for electric cooking, based on [30]

Charging of electric cars is not included in this profile and is therefore discussed in a separate section.

S.5.3.2. Electric car charging

In this research, a reasonable assumption on a charging pattern for home charging was made based on literature [31–33]. Besides, it is assumed that smart charging is an option in the near future [34] and therefore the evening charging peak is flattened and shifted from the evening to the night time. This results in the charging pattern in Figure 5.

The pattern shown here is only valid when a significant number of cars (>100) is charged simultaneously. When a car charges at home, it will charge with a capacity of 5.7 kW. However, smart charging of all cars together means that there will be a distribution in BEV charging, whereby cars will be charging alternately. Furthermore, a charging efficiency of 90.7% is applied [35]. To ensure variability over time, a noise of 20% is applied to the charging pattern.

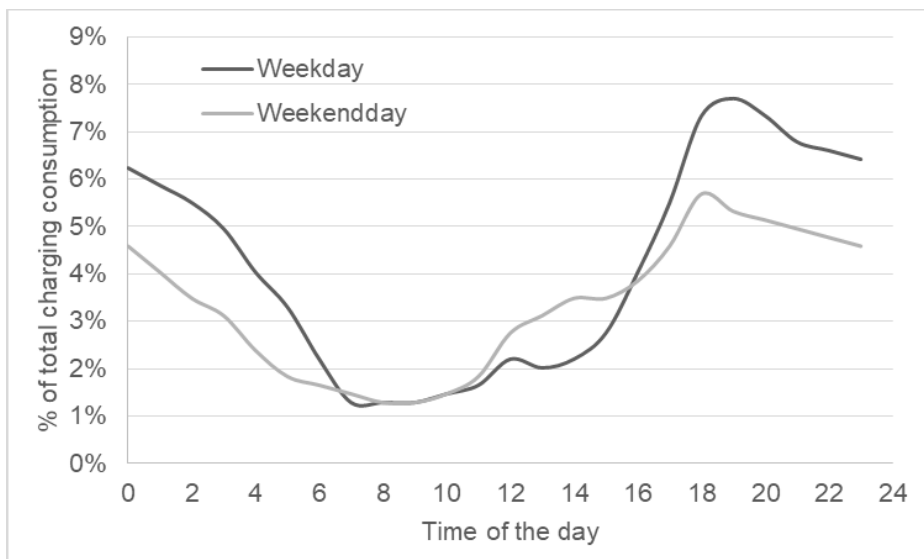


Figure 5 Charging pattern electric vehicles, based on [31–34].

Literature

1. IF Technoogy *Thermische Energie Uit Oppervlaktewater - Uitwerking van 13 Business Cases*; 2018; Available online: [http://waterenergie.stowa.nl/Upload/onderzoek_projecten/Thermische energie uit oppervlaktewater/TEO business case Fabriekskwartier Tilburg 20171101.pdf](http://waterenergie.stowa.nl/Upload/onderzoek_projecten/Thermische_energie_uit_oppervlaktewater/TEO_business_case_Fabriekskwartier_Tilburg_20171101.pdf).
2. Brolsma, R.; Boderie, P.; de Graaff, M.; Bonte, M.; Brand, R.; de Wit, J.; Hofman, J. Combining Water and Energy Supply. *Deltares* **2013**, 87.
3. HOMER Energy How HOMER Calculates the PV Array Power Output Available online: https://www.homerenergy.com/products/grid/docs/1.5/how_homer_calculates_the_pv_array_power_output.html (accessed on 21 November 2020).
4. Verkaik, J.W. *On Wind and Roughness over Land*; 2006; ISBN 9085043859.
5. Wood, J.; Gifford, J.; Arba, J.; Shaw, M. Production of Ultrapure Water by Continuous Electrodeionization. *Desalination* **2010**, 250, 973–976, doi:10.1016/j.desal.2009.09.084.
6. van der Roest, E.; Snip, L.; Fens, T.; van Wijk, A. Introducing Power-to-H3: Combining Renewable Electricity with Heat, Water and Hydrogen Production and Storage in a Neighbourhood. *Appl. Energy* **2020**, 257, doi:10.1016/j.apenergy.2019.114024.
7. Kopp, M.; Coleman, D.; Stiller, C.; Scheffer, K.; Aichinger, J.; Scheppat, B. Energiepark Mainz: Technical and Economic Analysis of the Worldwide Largest Power-to-Gas Plant with PEM Electrolysis. *Int. J. Hydrogen Energy* **2017**, 42, 13311–13320, doi:10.1016/j.ijhydene.2016.12.145.
8. IEA *The Future of Hydrogen*; Paris, 2019; Available online: <https://www.iea.org/publications/reports/thefutureofhydrogen/>.
9. Dorin Dorin Software 2018.
10. Ruhnau, O.; Hirth, L.; Praktiknjo, A. Time Series of Heat Demand and Heat Pump Efficiency for Energy System Modeling. *Sci. data* **2019**, 6, 189, doi:10.1038/s41597-019-0199-y.
11. Zuurbier, K.; van Dooren, T. *Urban Waterbuffer Spangen: Resultaten*; Nieuwegein, KWR 2019.111, 2019; Available online: <http://api.kwrwater.nl/uploads/2020/01/KWR-2019.111-Urban-Waterbuffer-Spangen-Resultaten.-Deelrapport-TKI-project-Urban-Waterbuffer.pdf>.
12. Juez-Larré, J.; van Gessel, S.; Dalman, R.; Remmelts, G.; Groenenberg, R. Assessment of Underground Energy Storage Potential to Support the Energy Transition in the Netherlands. *First Break* **2019**, 37, 57–66.
13. Caglayan, D.G.; Weber, N.; Heinrichs, H.U.; Linßen, J.; Robinius, M.; Kukla, P.A.; Stolten, D. Technical Potential of Salt Caverns for Hydrogen Storage in

- Europe. *Int. J. Hydrogen Energy* **2020**, *45*, 6793–6805, doi:10.1016/j.ijhydene.2019.12.161.
14. Pluijm, R. van der HyStock, *Connecting and Distributing Electrons and Molecules* 2018.
 15. Oldenbroek, V.; Verhoef, L.A.; van Wijk, A.J.M. Fuel Cell Electric Vehicle as a Power Plant: Fully Renewable Integrated Transport and Energy System Design and Analysis for Smart City Areas. *Int. J. Hydrogen Energy* **2017**, *42*, 8166–8196, doi:10.1016/j.ijhydene.2017.01.155.
 16. Langevin, C.D.; Thorne, D.T.; Dausman, A.M.; Sukop, M.C.; Guo, W. *SEAWAT Version 4: A Computer Program for Simulation of Multi-Species Solute and Heat Transport*; 2008;
 17. Langevin, C.D.; Shoemaker, W.B.; Guo, W. *MODFLOW-2000, the USGS Modular Groundwater Model - Documentation of the SEAWAT-2000 Version with Variable Density Flow Process and Integrated MT3DMS Transport Process*; 2003;
 18. Zheng, C.; Wang, P.P. *MT3DMS: A Modular Three-Dimensional Multispecies Transport Model for Simulation of Advection, Dispersion, and Chemical Reactions of Contaminants in Groundwater Systems; Documentation and User's Guide*; 1999;
 19. van der Roest, E.; Snip, L.; Bloemendal, M.; van Wijk, A. *Power-to-X; Nieuwegein, KWR* 2018.032, 2018; Available online: <https://library.kwrwater.nl/publication/56051448/>.
 20. IRENA *Electricity Storage and Renewables: Costs and Markets to 2030*; 2017; Available online: <https://www.irena.org/publications/2017/Oct/Electricity-storage-and-renewables-costs-and-markets>.
 21. Mongird, K.; Viswanathan, V.; Balducci, P.; Alam, J.; Fotedar, V.; Koritarov, V.; Hadjerioua, B. *Energy Storage Technology and Cost Characterization Report I Department of Energy*; 2019; Available online: <https://www.energy.gov/eere/water/downloads/energy-storage-technology-and-cost-characterization-report>.
 22. Standardization, E.C. for NEN-EN 13941-1 - District Heating Pipes - Design and Installation of Thermal Insulated Bonded Single and Twin Pipe Systems for Directly Buried Hot Water Networks. **2016**.
 23. EnergiNet; The Danish Energy Agency *Technology Data - Generation of Electricity and District Heating*; 2020; Available online: <https://ens.dk/en/our-services/projections-and-models/technology-data/technology-data-generation-electricity-and>.
 24. Hydrogen Europe *Vision on the Role of Hydrogen and Gas Infrastructure on the Road Toward a Climate Neutral Economy - A Contribution to the Transition of the Gas Market*; 2019; Available online: [https://www.hydrogeneurope.eu/sites/default/files/2019_Hydrogen Europe Vision on the role of Hydrogen and Gas Infrastructure.pdf](https://www.hydrogeneurope.eu/sites/default/files/2019_Hydrogen%20Europe%20Vision%20on%20the%20role%20of%20Hydrogen%20and%20Gas%20Infrastructure.pdf).

25. Hydrogen Council *Path to Hydrogen Competitiveness - A Cost Perspective*; 2020; Available online: https://hydrogencouncil.com/wp-content/uploads/2020/01/Path-to-Hydrogen-Competitiveness_Full-Study-1.pdf.
26. Hermkens, R.; Jansma, S.; van der Laan, M.; de Laat, H.; Pilzer, B.; Pulles, K. *Toekomstbestendige Gasdistributienetten*; 2018; Available online: <https://www.netbeheernederland.nl/nieuws/huidige-gasnet-geschied-ge-maken-voor-waterstof-1240>.
27. Asadullah, M. Biomass Gasification Gas Cleaning for Downstream Applications: A Comparative Critical Review. *Renew. Sustain. Energy Rev.* **2014**, *40*, 118–132, doi:10.1016/j.rser.2014.07.132.
28. NEDU Verbruiksprofielen - User Profiles Electricity 2018 Available online: <https://www.nedu.nl/documenten/verbruiksprofielen/> (accessed on 26 November 2020).
29. CE Delft *Elektrisch Koken*; 2018; Available online: https://www.ce.nl/assets/upload/image/Plaatjes_themapagina's/Duurzame_stad/Factsheet_Elektrisch_koken_DEF.pdf.
30. van Melle, T.; Menkveld, M.; Oude Lohuis, J.; de Smidt, R.; Terlouw, W. *De Systeemkosten van Warmte Voor Woningen*; 2015; Available online: <http://resolver.tudelft.nl/uuid:9d49b1d3-107b-4f49-a36c-b606786bc207>.
31. Movares *Laadstrategie Elektrisch Wegvervoer*; 2013; Available online: https://www.netbeheernederland.nl/_upload/Files/Elektrisch_vervoer_11_ccede3d2ae.pdf.
32. RVO *Special: Laadgedrag van Nederlandse Elektrische Rijders*; 2014; Available online: <https://nederlandelektrisch.nl/u/files/special-laadgedrag.pdf>.
33. Sadeghianpourhamami, N.; Refa, N.; Strobbe, M.; Develder, C. Quantitative Analysis of Electric Vehicle Flexibility: A Data-Driven Approach. *Int. J. Electr. Power Energy Syst.* **2018**, *95*, 451–462, doi:10.1016/j.ijepes.2017.09.007.
34. Gerritsma, M.K.; AlSkaif, T.A.; Fidler, H.A.; Sark, W.G.J.H.M. van Flexibility of Electric Vehicle Demand: Analysis of Measured Charging Data and Simulation for the Future. *World Electr. Veh. J.* **2019**, *10*, 14, doi:10.3390/wevj10010014.
35. Farahani, S.S.; Bleeker, C.; van Wijk, A.; Lukszo, Z. Hydrogen-Based Integrated Energy and Mobility System for a Real-Life Office Environment. *Appl. Energy* **2020**, *264*, 114695, doi:10.1016/j.apenergy.2020.114695.